

1 **Title:** Black carbon concentrations and modeled smoke deposition fluxes to the bare ice dark
2 zone of the Greenland Ice Sheet

3 **Authors:** Alia L. Khan¹, Peng Xian², Joshua Schwarz³

4 ¹Department of Environmental Sciences, Western Washington University

5 ²Aerosol and Radiation Section of the Marine Meteorology Division, Naval Research
6 Laboratory, Monterey, California, USA

7
8 ³Chemical Sciences Division, NOAA Earth System Research Laboratory (ESRL), Boulder, CO,
9 United States

10

11 **Correspondence to:** Alia L. Khan (alia.khan@wwu.edu)

12

13 **Abstract:**

14 Ice-albedo feedbacks in the ablation region of the Greenland Ice Sheet (GrIS) are difficult to
15 constrain and model due in part to our limited understanding of the seasonal evolution of the
16 bare-ice region. To help fill observational gaps, 13 surface samples were collected on the GrIS
17 across the 2014 summer melt season from patches of snow that were visibly light, medium, and
18 dark colored. These samples were analyzed for their refractory black carbon (rBC)
19 concentrations and size distributions with a Single Particle Soot Photometer coupled to a
20 characterized nebulizer. We present a size distribution of rBC in fresh snow on the GrIS, as well
21 as from surface hoar in the bare ice dark zone of the GrIS. The size distributions from the
22 surface hoar samples appear unimodal, and were overall smaller than the fresh snow sample,
23 with a peak around 0.3 μm . The fresh snow sample contained very large rBC particles that had a
24 pronounced bimodality in peak size distributions, with peaks around 0.2 μm and 2 μm . rBC
25 concentrations ranged from a minimum of 3 $\mu\text{g-rBC/L-H}_2\text{O}$ in light-colored patches at the
26 beginning and end of the melt season, to a maximum of 32 $\mu\text{g-rBC/L-H}_2\text{O}$ in a dark patch in
27 early August. On average, rBC concentrations were higher ($20 \mu\text{g-rBC/L-H}_2\text{O} \pm 10 \mu\text{g-rBC/L-}$

28 H₂O) in patches that were visibly dark compared to medium patches (7 μg-rBC/L-H₂O ± 2 μg-
29 rBC/L-H₂O) and light patches (4 μg-rBC/L-H₂O ± 1 μg-rBC/L-H₂O), suggesting BC aggregation
30 contributed to snow aging on the GrIS, and vice versa. Additionally, concentrations peaked in
31 light and dark patches in early August, which is likely due to smoke transport from wildfires in
32 Northern Canada and Alaska as supported by the Navy Aerosol Analysis and Prediction System
33 (NAAPS) reanalysis model. According to model output, 26 mg/m³ of biomass burning derived
34 smoke was deposited between April 1st and August 30th, of which 85% came from wet
35 deposition and 67% was deposited during our sample collection timeframe. The increase in rBC
36 concentration and size distributions immediately after modelled smoke deposition fluxes suggest
37 biomass burning smoke is a source of BC to the dark zone of the GRIS. Thus, the role of BC in
38 the seasonal evolution of the ice-albedo feedback should continue to be investigated in the bare-
39 ice zone of the GrIS.

40

41 **1. Introduction**

42 The bare ice dark zone of the southwest Greenland Ice Sheet (GrIS) is characterized by low
43 albedo due in part to the presence of light absorbing impurities (LAIs), that create a positive ice-
44 albedo feedback through increased surface melting, ice grain growth, and darkening (Tedesco et
45 al., 2016). LAIs in this region are a mixture of cryoconite, ice algae (Stibal et al., 2017; Ryan et
46 al., 2018), dust (Wientjes et al., 2011), and black carbon (BC) such as from Northern
47 Hemisphere fires (Khan et al., 2017), yet the relative contribution of each light absorbing particle
48 is still uncertain. The radiative forcing of these LAIs, along with warming summer surface
49 temperatures (Hanna et al., 2008), leads to large volumes of supra-glacial melt (Greuell, 2000).

50 Furthermore, retreat of the snowline is amplifying surface melt of the GrIS due to increased bare
51 ice exposure (Ryan et al., 2019) and the LAI-ice albedo feedbacks described above.

52 BC in and on snow and ice is known to warm the Arctic and contribute to snow and ice
53 melting, however the magnitude of its influence is still highly uncertain e.g., (Flanner et al.,
54 2007; Bond et al., 2013). BC concentration in air is typically operationally defined depending on
55 the analytical technique used (Petzold et al., 2013). Many in-situ measurements of BC
56 concentration in snow in the Arctic have been reported by the Integrating Plate and Integrating
57 Sandwich (IS) technique, which provides analysis of light absorption of particulate impurities
58 through spectrophotometric analysis of filter loaded with particulates collected from melted
59 samples (e.g., Clarke and Noone, 1985; Doherty et al., 2010; Doherty et al., 2013). Doherty et al.
60 (2010) reported a median concentration of 3 ng/g in surface snow, with higher concentration
61 layers up to ~20ng/g in snow profiles at Dye 2. Snow samples from snowpits in the northwest
62 sector of the GrIS were also collected in 2013 and 2014 from two traverses and analyzed for
63 elemental/organic carbon (EC/OC). The mean concentration of the samples collected was 2.6
64 ng/g and the mean peak was 15 ng/g. Based on these results, it was determined that EC/OC do
65 not influence the snow albedo in the NW sector of the GrIS dry zone (Polashenski et al., 2015a).
66 Observations of refractory black carbon (rBC) analyzed by the Single Particle Soot Photometer
67 (SP2) have been published from snow profiles and ice cores in the accumulation region closer to
68 the Summit research station (McConnell et al., 2007a; Keegan et al., 2014b; Lim et al., 2014).
69 McConnell et al. (2007) presented BC concentrations from a 215-year ice-core record collected
70 at D4 in West Central Greenland with average concentrations of 1.7ng/g in pre-industrial times,
71 2.3ng/g over the period 1950-2002, and around 5 ng/g in the peak period of the early 1900s. The
72 maximum monthly concentration observed was 58.8 ng/g in 1854, however, monthly

73 concentrations only exceeded 5 ng/g ~2-3 times each decade after 1950. Polashenski et al.,
74 (2015) provides a comprehensive review of previous BC concentrations in their supplemental
75 info, showing that the BC average ranges between 1.5 and 3 ng/g over an annual cycle, with peak
76 deposition occurring during summer episodic events, with concentrations of 5 - 10+ ng/g only
77 occurring a few times at a given site per decade. Similarly, rBC concentrations from the
78 percolation zone of the GrIS have been shown to be relatively low, less than 1.5 ng/g (Lewis et
79 al., 2021).

80 rBC measured by SP2 has been shown to provide more reliable measurements of
81 concentration than the IS or EC/OC (from liquid and air samples, respectively) techniques
82 because it is largely free from the interference of materials other than rBC (Kondo et al., 2011;
83 Schwarz et al., 2012) such as pyrolyzed organic carbon artifacts (Lim et al., 2014). It also
84 provides a lower detection limit and increased sensitivity at low concentrations (Lim et al. 2014).
85 The SP2 coupled with a nebulizer also provides a measurement of rBC particle size distribution
86 from liquid samples.

87 rBC particle size has been observed in some snow samples to be larger than expected
88 from atmospheric measurements, reflecting to some degree size-dependent removal processes
89 from the atmosphere (Schwarz et al., 2013). The rBC size distribution in snow, which at this
90 point is constrained by direct observations not supported by detailed modeling, is a significant
91 source of uncertainty for calculating the overall radiative forcing of BC-in-snow on the Arctic
92 climate, as well as the global climate (e.g., Bond et al., 2013). Very few rBC size distributions in
93 snow have been reported globally, with most measurements coming from the Arctic (Lim et al.,
94 2014; Khan et al., 2017; Mori et al., 2019).

95 Although, observations of BC in snow have been previously observed in the percolation zone
96 (Dye 2) and accumulation zone (Summit Station) by the IS technique (Doherty et al., 2010a, 2013)
97 and rBC-SP2 at Summit Station (McConnell et al., 2007b; Keegan et al., 2014a; Lim et al., 2014),
98 to the authors' knowledge, no reports of rBC concentrations with size distributions in snow and
99 surface hoar have been reported from the GrIS, providing new insight, particularly into the
100 dynamic bare-ice region.

101 Here we present rBC concentrations with size distributions from the bare ice region of the
102 GrIS before and after influence by a major wildfire event, along with NAAPS modelled wet and
103 dry deposition. Our findings suggests that rBC surface hoar concentrations in the bare ice zone
104 reflect atmospheric conditions momentarily, before being reset, possibly by supra-glacial melt.
105 Additionally, NAAPS model output suggest most of the biomass burning derived smoke
106 deposition comes in the form of wet removal (i.e., removal by precipitation). These rBC
107 concentrations and size distributions provide insight into the seasonal evolution of impurities,
108 which are needed to constrain ice-albedo feedbacks in the bare-ice zone of the GrIS.

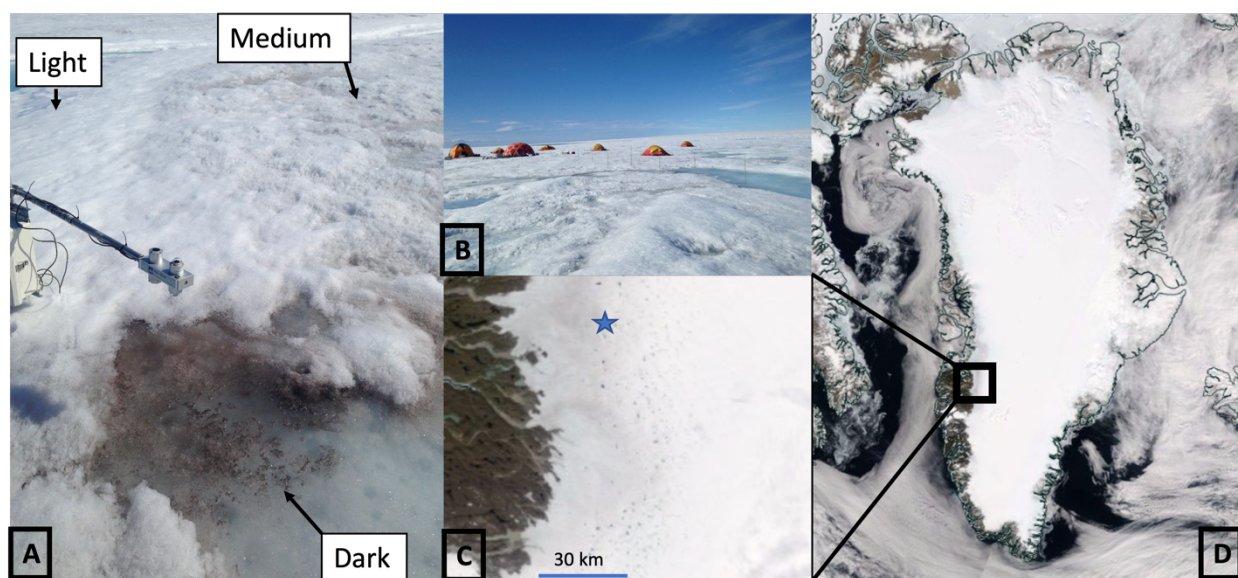
109

110 **2. Methods**

111 *2.1 Site Description and Snow Sampling*

112 The field site was in the southwestern region of the GrIS near the S6 automated weather station
113 at 67 04.779°N, 49 24.077°W, and 1011 m above sea level. More information on the study site
114 can be found in Stibal et al. (2017). A fresh snow surface sample (2 – 3 cm), was collected just
115 after a snow event on 2014-06-27. Three surface hoar samples (2 – 3 cm), were collected in 150
116 mL pre-cleaned and combusted amber glass bottles four times between 2014-06-28 and 2014-08-
117 11 across the 2014 summer melt season from visually identified light, medium, and dark patches

118 of surface hoar, for a total of 13 samples, including the fresh snow. While all sample sites could
119 include a mixture of ice algae, dust, black carbon (i.e, cryoconite), the dark patches especially
120 could represent refrozen melt that is enhanced in LAIs, including rBC. A mixture of light,
121 medium and dark 1 – 3 m² patches were sampled within the ~.5 km² study area to characterize
122 the breadth of surface types and heterogenous distribution of impurities. Samples were stored
123 frozen in a ‘field cooler’ dug into the ice and then transported frozen on ice to Kangerlussuaq,
124 and shipped on dry ice to the Denver Airport, and then transported immediately to a freezer at
125 the Institute of Arctic and Alpine Research (INSTAAR) at the University of Colorado – Boulder.



126 A and B are images collected by Dr. Alia Khan. C and D are MODIS satellite images acquired from the NASA Worldview application.

127 **Figure 1:** A) Example light, medium and dark patches of ice. B) The Dark Snow Field Camp. C)
128 The southwest GrIS dark zone with the field sampling location indicated by a blue star and D)
129 the GrIS from MODIS on July 2nd, 2014.

130

131 *2.2 Processing for Refractory Black Carbon*

132 The samples were transported frozen from INSTAAR to the Earth System Research Laboratory
133 at the National Oceanic and Atmospheric Administration where they were analyzed for rBC

134 mass mixing ratios (MMRs) by SP2 coupled to a nebulizer per the methods described in Katich
135 et al. (2017) and Khan et al. (2018). Briefly, the samples were melted for the first time just prior
136 to analysis with the SP2 and aerosolized with a carefully calibrated concentric pneumatic
137 nebulizer based on a customized U5000 AT+ nebulizer (Teledyne Cetac, Inc.) which the
138 ultrasonic piezo was replaced with a concentric pneumatic nebulizer. The SP2 was calibrated
139 with fullerene soot (Lot# F12S011, Alfa Aesar Inc., Wood Hill, MA) with the community
140 calibration approach (Baumgardner et al., 2012) over masses of 1 – 20 fg. Using a power law
141 calibration dependence following Schwarz et al., [2012], the resulting linear calibration of SP2
142 signal to rBC mass applied to mass of 80 fg was extended further to 4000 fg. The SP2 was
143 operated with a widely staggered gain for two incandescent channels, allowing sizing of rBC
144 mass in the range $\sim 1 - 4000$ fg.

145 Melted snow samples were interspersed with deionized water blanks to confirm a low
146 background, especially relative to the MMRs, indicating no appreciable contamination to
147 concentrations and size distributions. Little size-dependence in nebulization efficiency was
148 confirmed with concentration standards of polystyrene latex spheres (PSLs) over 220 – 1500 nm
149 diameter, which is consistent with recent results from concentric pneumatic nebulizers (Wendl et
150 al., 2014, Katich et al., 2017). Therefore, size dependent corrections were not necessary. During
151 data acquisition with the SP2, its lower mass-detection limit was 1.2 fg, which corresponds to
152 about a 110 nm volume equivalent diameter (VED) size detection limit, assuming 1.8g/cc void
153 free density. A 510 nm diameter PSL concentration standard was sampled between melted snow
154 analyses to track possible changes in nebulization efficiency during each day of sampling. This
155 revealed effectively constant efficiency varying with a standard deviation less than 5%. A
156 gravimetric mass concentration standard (Schwarz et al., 2012) was also used to evaluate

157 nebulization efficiency. The results of the PSL and gravimetric calibrations of nebulizer
158 efficiency were consistent within uncertainties of 20% and were averaged to provide a best-
159 estimate nebulization efficiency that was then used to produce the BC MMR values as in
160 Schwarz et al. (2012).

161

162 *2.3 Global Aerosol Modeling*

163 The Navy Aerosol Analysis Prediction System (NAAPS) model is a global aerosol transport
164 model which provides 6-hrly biomass burning smoke, anthropogenic and biogenic fine aerosols,
165 dust, and sea salt aerosol forecasts and analyses below 100 hPa at 1/3° latitude/longitude spatial
166 resolution and contains 42 vertical atmospheric levels. The NAAPS reanalysis (NAAPS-RA) is
167 available 2003-current with a coarser spatial resolution (1° latitude/longitude horizontal and 25
168 vertical levels) (Lynch et al., 2016). Total column aerosol optical thickness (AOT) is constrained
169 through assimilation of quality-controlled satellite AOT retrievals from the Moderate Resolution
170 Imaging Spectroradiometer (MODIS) and Multi-angle Imaging SpectroRadiometer (MISR).
171 Near-real time satellite based thermal anomaly data enables detection of wildfires and
172 construction of biomass burning smoke emissions (Reid et. al., 2009). Orbital corrections for
173 MODIS-based fire detections and regional factors were applied on emissions so that the
174 reanalysis AOT verifies well with ground-based measurements (Lynch et al., 2016). The
175 NAAPS-RA has been applied to a broad range of science applications, and specifically the life
176 cycle, climatology, radiative forcing, aerosol-atmosphere-ice-ocean interactions of biomass
177 burning smoke aerosols (e.g., Reid et al., 2012; Xian et al., 2013; Markowicz et al., 2021; Ross et
178 al., 2018; Khan et al., 2019; Carson-Marquis et al., 2021), as well as previously to corroborate
179 wildfire smoke transport to the GrIS (Khan et al., 2017), Arctic Canada (Ranjbar et al., 2019),

180 Svalbard (Markowicz et al., 2016; 2017), the pan-Arctic region (Xian et al., 2022a, b), the
181 Nepalese Himalayas (Khan et al., 2020), and the Antarctic (Khan et al., 2018; Khan et al., 2019).
182 Speciated AOT, surface aerosol concentration and deposition flux are used in this study. Here the
183 deposition is calculated as 24-hour flux to the surface of the ice sheet in $\text{mg}/\text{m}^2/\text{day}$. Estimating
184 atmospheric properties related to biomass burning is highly complex and is influenced by wide
185 variety of factors such as the type of fuel, combustion temperature, and atmospheric
186 conditions. Also, the chemical, optical and physical properties of biomass burning aerosols can
187 change during atmospheric transport and dispersion. The mass ratio of rBC to total mass in
188 biomass burning smoke particles is estimated to be 5–10% black carbon in the NAAPS-RA
189 model based on field studies (see a summary in Reid et al., 2005) and here we chose 7% as a
190 median value.

191 **3. Results and Discussion**

192 *3.1 rBC Concentrations*

193 rBC concentrations in the surface hoar ranged from a minimum of $3 \mu\text{g-rBC}/\text{L-H}_2\text{O}$ in light
194 patches at the beginning and end of the melt season, to a peak of $32 \mu\text{g-rBC}/\text{L-H}_2\text{O}$ in a dark
195 patch in early August (Table 1). rBC concentrations were higher in patches that were visibly
196 darker ($20 \mu\text{g-rBC}/\text{L-H}_2\text{O}$) compared to medium patches ($7 \mu\text{g-rBC}/\text{L-H}_2\text{O}$) and light patches (4
197 $\mu\text{g-rBC}/\text{L-H}_2\text{O}$), suggesting BC aggregates with dust and biological material on the GrIS. Light
198 and dark patch concentrations peaked in early August. Our minimum concentrations are in the
199 range of rBC concentrations found elsewhere on the GrIS, but our peaks are higher than
200 previously reported concentrations from snow on the GrIS (Doherty et al., 2010a; Polashenski et
201 al., 2015; Lewis et al., 2021). Our maximum concentrations are higher than the highest
202 concentrations observed in vertical snow with the IS (Doherty et al., 2010b) and EC/OC

203 technique (Polashenski et al., 2015), but less than the highest monthly average concentration of
 204 year of 1854 reported in an ice core by McConnell et al. (2007). The concentration of rBC in the
 205 fresh snow (3 $\mu\text{g-rBC/L-H}_2\text{O}$) sample was roughly the same as the light surface hoar patches on
 206 2014-06-28 and 2014-08-11.

207

208 **Table 1:** NAAPs Smoke Dry, Wet, and Total Deposition ($\text{mg/m}^2/\text{day}$) from April 1st prior to
 209 sample collection. Average rBC concentrations from visually light, medium, and dark patches of
 210 surface hoar. All samples were collected at 67.07979701 degrees N and -49.40116603 degrees W
 211 at 1005 meters above sea level in the dark zone ablation region of the SW Greenland Ice Sheet.

212 ^The fresh snow sample is a single sample.

Date	NAAPS	NAAPS	NAAPS	Average	Snow type (visual color)	rBC $\mu\text{g-rBC/L-H}_2\text{O}$
	Smoke Dry Deposition ($\text{mg/m}^3/\text{day}$)	Smoke Wet Deposition ($\text{mg/m}^3/\text{day}$)	Smoke Total Deposition ($\text{mg/m}^2/\text{day}$)	rBC $\mu\text{g-rBC/L-H}_2\text{O}$		
6/27/14	0.58	1.98	2.56	3.05 [^]	Fresh	3.05
6/28/14	0.60	6.92	7.51	8.37	Light	2.87
					Medium	9.61
					Dark	12.62
7/21/14	0.75	6.93	7.69	11.45	Light	4.21
					Medium	6.42
					Dark	23.71
8/2/14	1.51	9.44	10.95	14.15	Light	5.27
					Medium	4.71
					Dark	32.47
8/11/14	1.94	12.14	14.08	8.12	Light	2.96

Medium	8.75
Dark	12.64

213

214 *3.2 rBC Size Distributions*

215 We found very large rBC are present (Figure 2A, B and C), especially in the fresh snow sample.

216 The large size distribution in fresh snow follows previous findings in the rocky mountains that

217 rBC size distributions can be larger in surface snow than expected in aerosol in the atmosphere

218 (Schwarz et al., 2013). Furthermore, the fresh event is associated with a more pronounced

219 bimodality at $\sim 0.2 \mu\text{m}$ and $2 \mu\text{m}$ (Figure 2A), whereas the rBC in surface hoar samples appears

220 more unimodal (Figure 2B and 2C). The average surface hoar rBC sizes, which have not been

221 previously reported in the literature, are smaller than the one fresh snow sample with a peak

222 around $0.3 \mu\text{m}$. This is still larger than typical modal sizes for rBC observed in the atmosphere

223 (in the range $\sim 0.11 - 0.2 \mu\text{m}$ typically). Furthermore, no apparent patterns emerge in the size

224 distributions across the light, medium and dark patches over the duration of the season.

225 However, the surface hoar rBC size distributions likely evolve, just as the seasonal snow cover

226 evolves into bare ice and surface hoar, but we are unable to assess from this relatively small data

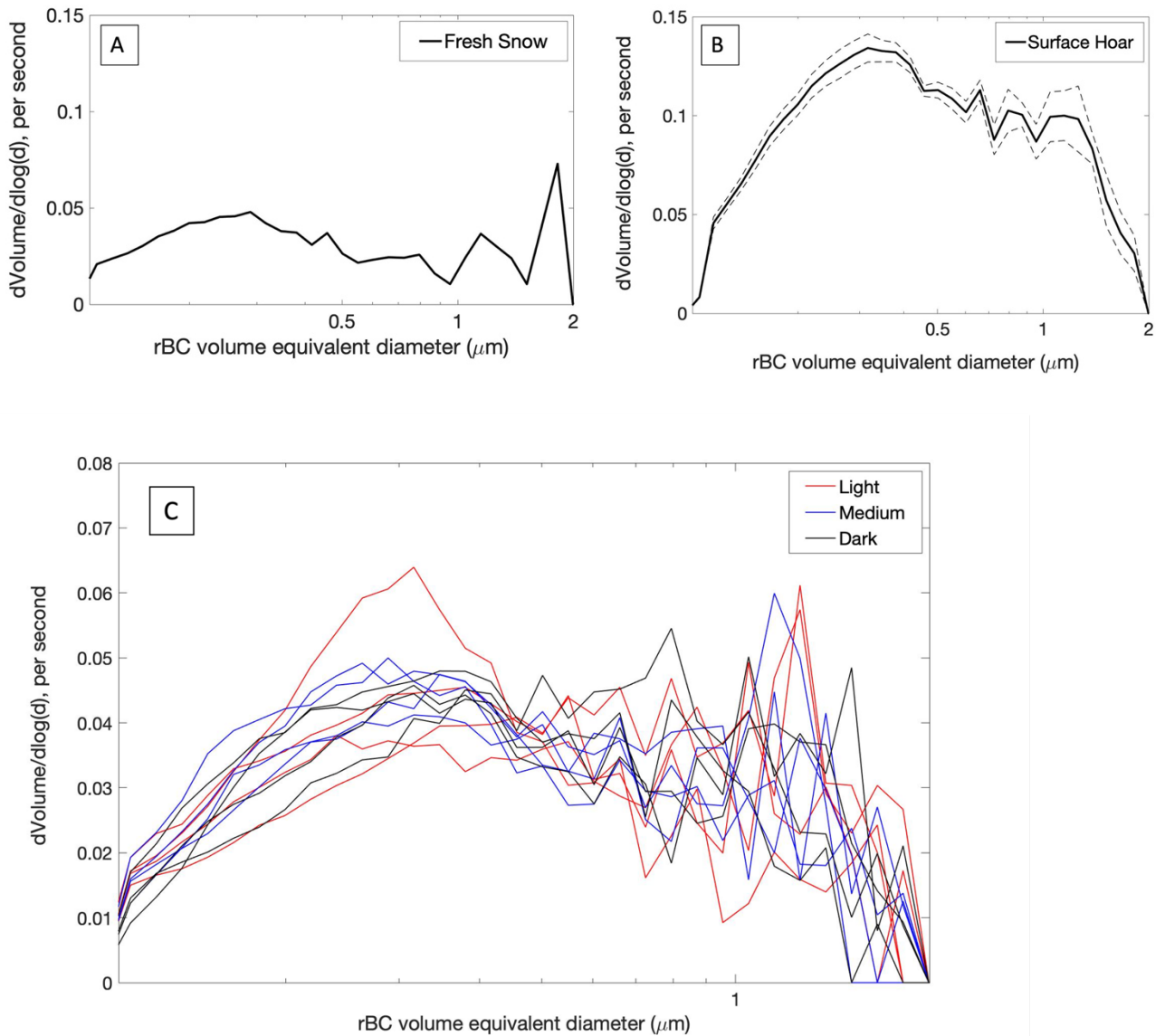
227 set. This conjecture is supported by observations that repeated freeze/thaw cycles tend to cause

228 rBC coagulation in liquid (Schwarz et al., 2013). Regardless, these initial results of rBC size

229 distributions from fresh snow and surface hoar in the bare ice region of the GrIS are important

230 for informing ice-albedo models, which are still being developed and refined for bare ice regions

231 of the ice sheet (e.g. Flanner et al., 2007).



232

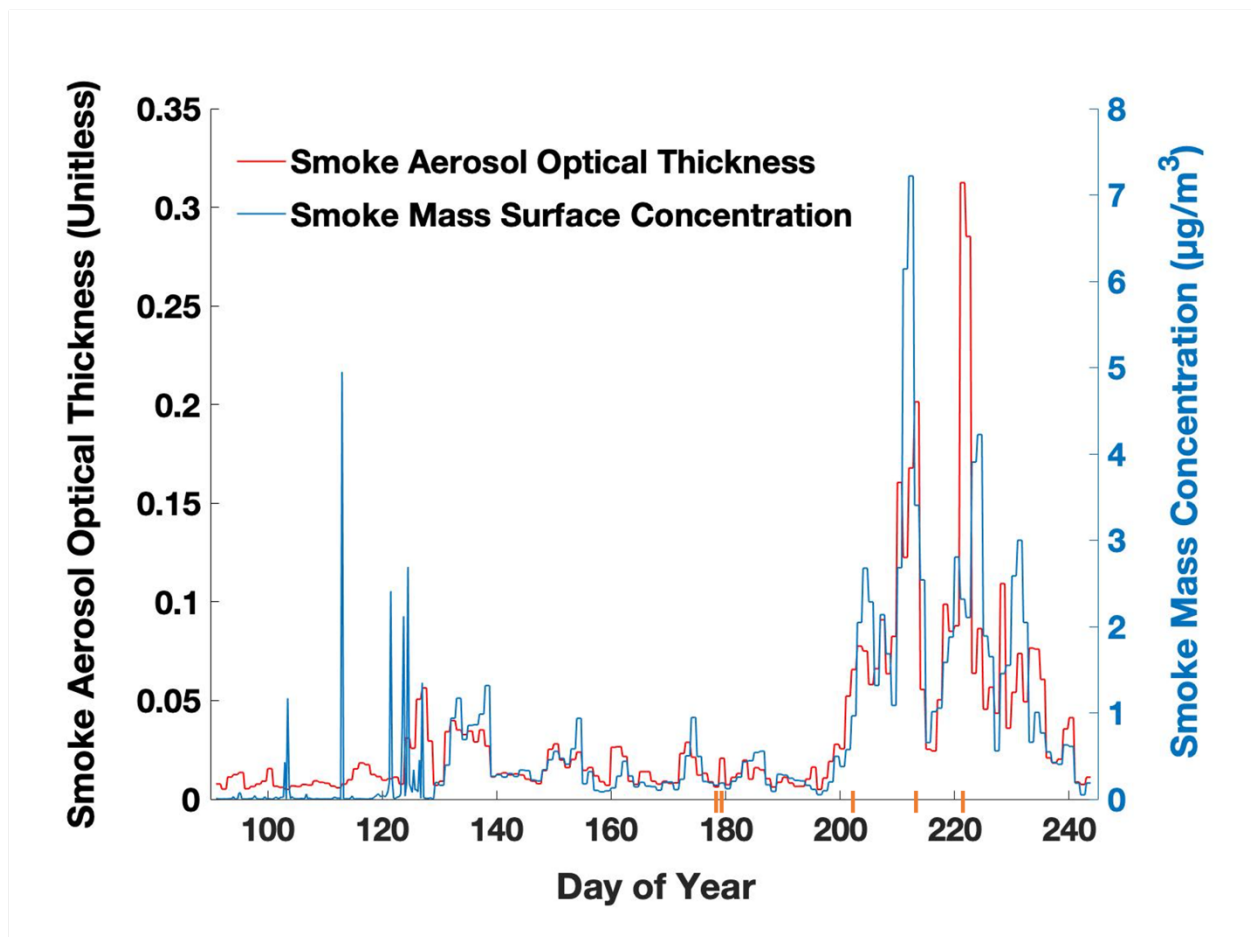
233

234 **Figure 2:** A) rBC size distribution of fresh snow (n=1), B) all surface hoar samples over the
 235 duration of the season (n=12) and C) the size distribution of each surface hoar sample
 236 categorized as light, medium and dark. The dashed lines in Figure 2B represent the max and min
 237 size distributions and the solid black line is the average.

238

239 *3.3 NAAPS Aerosol Model Comparison and Evaluation*

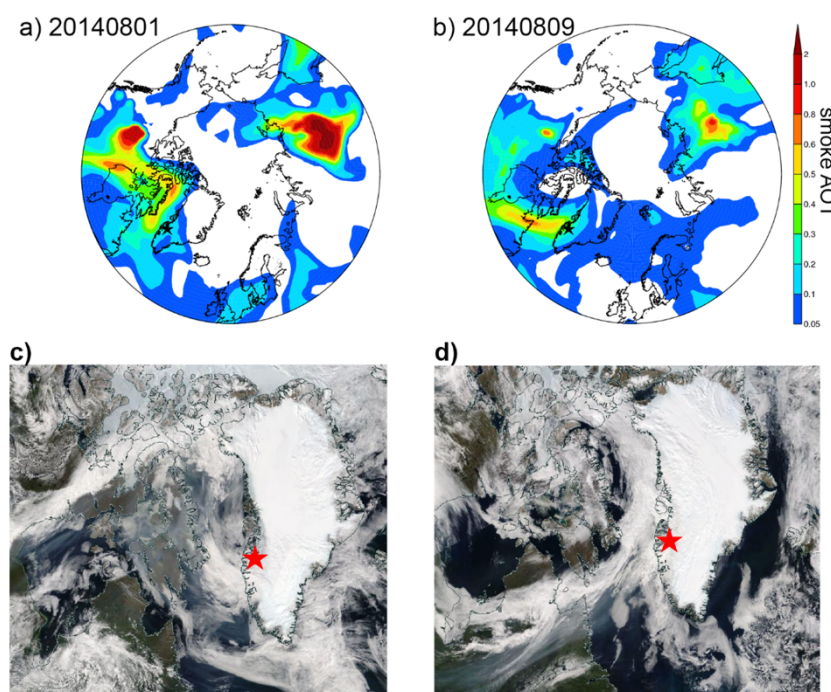
240 The ground observations were then compared to cumulative aggregates of smoke deposition
241 fluxes modelled with the Navy Aerosol Analysis Prediction System reanalysis model. AOT
242 derived from MODIS and modeled by NAAPS demonstrates that a large wildfire smoke event
243 was observed just before the third sample was collected and during the time the fourth sample
244 was collected (Figure 3). Concomitant AOT and surface concentration predictions from the
245 NAAPS model confirms our peak concentrations are likely due to Northern Hemisphere wildfire
246 smoke (Figure 4 A- D).
247



248

249 **Figure 3:** Aerosol optical thickness (AOT) derived from NAAPS reanalysis

250 over the sampling season from smoke and dust. B) Smoke mass concentration ($\mu\text{g}/\text{m}^3$) in the
251 surface layer of the model (centered around 16m). The five sampling dates are marked in orange.



252
253 **Figure 4:** Biomass burning smoke transport reaching the GrIS from the west based on NAAPS-
254 RA daily-mean smoke AOT and MODIS TERRA true color imageries for **A and C)** Aug. 1,
255 2014 and **B and D)** Aug. 9, 2014. The sampling location is marked with a black star in the
256 NAAPS-RA plots (A and B), and red stars in the MODIS imageries (C and D).

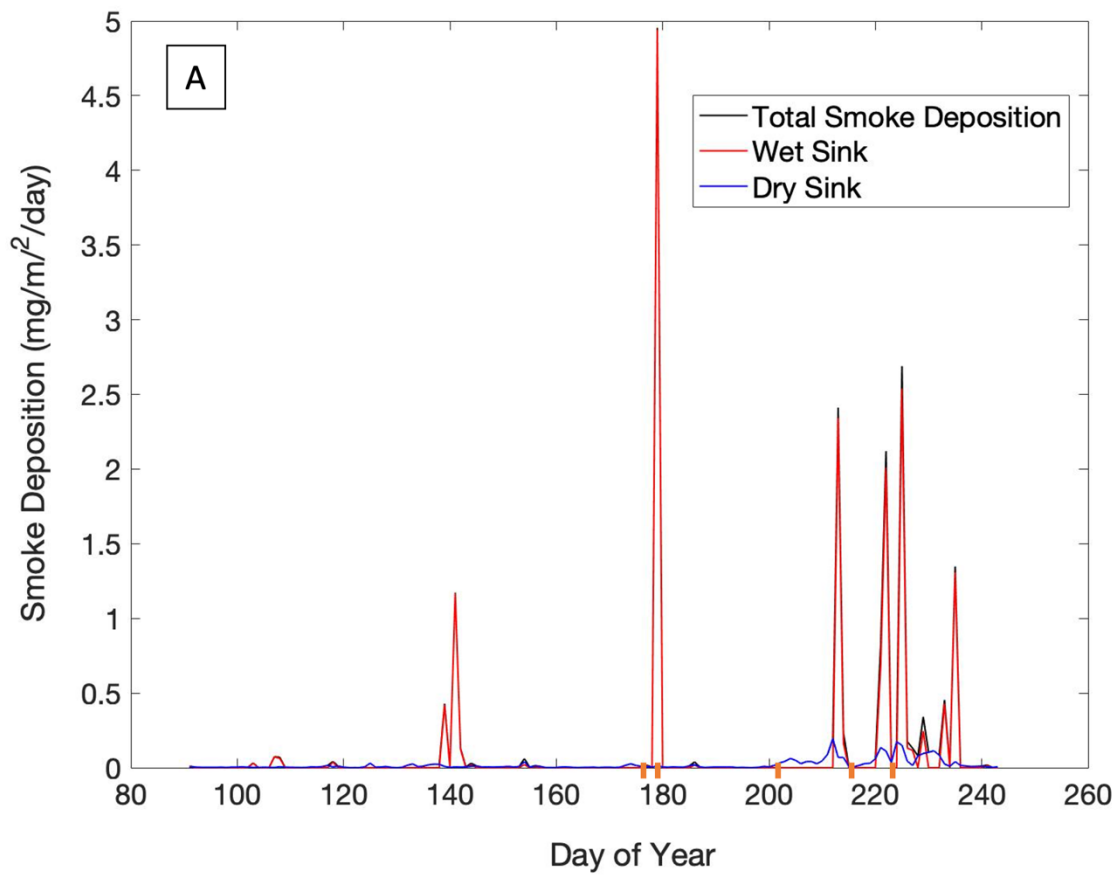
257 According to NAAPS model output, the deposition flux of smoke (Table 1 and Fig. 5)
258 onto the ice surface of the dark zone during our model study period, April 1st – August 30th, was
259 25.6 $\text{mg}/\text{m}^2/\text{day}$ and 85% came from wet deposition. April 1st to August 30th was chosen based
260 on the primary Northern Hemisphere wildfire season and smoke transport to the Arctic (Xian et
261 al., 2022b). 68% of this smoke ($17.3 \text{ mg}/\text{m}^2/\text{day}$) was deposited during our sample collection
262 period from June 27th to August 11th. Prior to the first sample collected on June 27th, 10% of the
263 total smoke flux ($2.6 \text{ mg}/\text{m}^2/\text{day}$) was deposited from April 1st to June 26th. After the last sample
264 was collected on August 11th, $5.8 \text{ mg}/\text{m}^2/\text{day}$ of smoke was deposited between August 12th and
265 30th.

266 We evaluate the NAAPS-RA deposition flux based on the rBC concentration observed in
267 fresh snow, which was 3 $\mu\text{g-rBC/L-H}_2\text{O}$. The NAAPS model assumes 7% of smoke is BC. The
268 snow event that preceded the fresh snow sample collection, had a modeled precipitation rate of
269 10 mm/day or 10 L/m². The modeled smoke deposition flux is 3000 $\mu\text{g/m}^2/\text{day}$ or 300 $\mu\text{g/L}$ over
270 24 hours. At 7% BC of total smoke, that leaves us with 21 $\mu\text{g-BC/L-H}_2\text{O}$. Therefore, the model
271 appears to be off by roughly a factor of 7 for this one snow sample. Continued work is in
272 progress to evaluate the model across a larger sample size of rBC ground observations across the
273 Arctic.

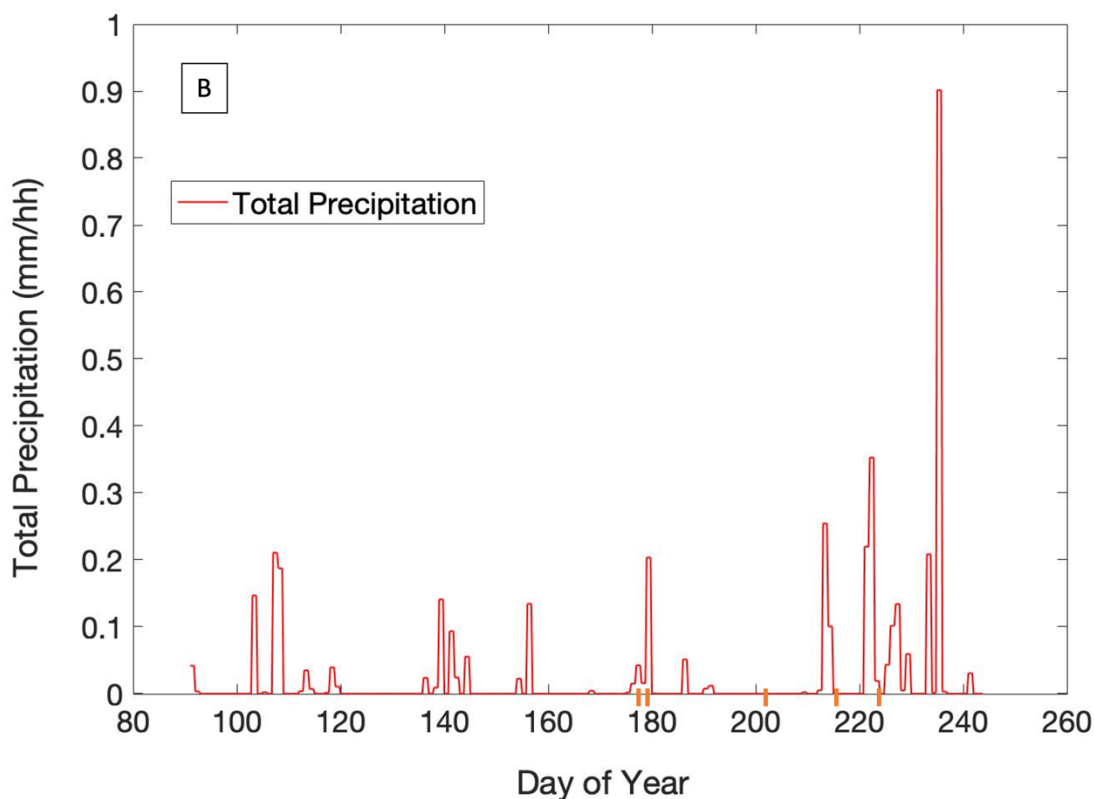
274 Two case studies of interest arise in the modelled total NAAPS smoke flux when
275 comparing wet and dry deposition. The first one is a large wet deposition flux and the second is a
276 considerable dry deposition flux. The first wet deposition flux occurred between June 27th and
277 28th (day of year 178 and 179), during a snow event (Fig. 5A and B). Here we see the largest
278 increase in the total deposition flux of smoke over the study period at 5.0 $\text{mg/m}^3/\text{day}$ in just over
279 24 hours. 99.8% of this comes from wet deposition. When we compare these model findings to
280 the observational rBC data in the surface hoar and snow, we see the rBC concentration in fresh
281 snow, 3 $\mu\text{g-rBC/L-H}_2\text{O}$, is high compared to pristine fresh snow previously found in Svalbard, 1
282 $\mu\text{g-rBC/L-H}_2\text{O}$ (Khan et al., 2017). The average rBC concentration across the light, medium and
283 dark patches is also relatively high for a non-human impacted site in the polar regions (Cordero
284 et al., 2022). A previous study of black carbon in supra-glacial melt from the same GRIS site
285 previously confirmed the dissolved BC molecular signature was indicative of wildfire smoke that
286 likely came from Northern Canada and Alaska (Khan et al., 2017). Between July 22nd and
287 August 2nd, the model again shows a large proportion of the total deposition flux coming from
288 wet deposition, 77% of the 3.2 $\text{mg/m}^2/\text{day}$. Similarly, from August 3rd to 11th, 86% of the 3.1

289 mg/m³/day smoke deposition flux was from wet deposition (Fig. 5A). Again, this follows an
290 increase in the total precipitation (Fig. 5B).

291 However, a dry deposition case arises on July 21st, 2014 (DOY 172). Here the NAAPS
292 model does not produce a large total smoke deposition flux, but the rBC concentrations are still
293 relatively high. Since the previous sampling event on June 28th (DOY 179), the model produces
294 0.2 mg/m³/day total deposition flux, where only 16% comes from wet deposition. The majority,
295 84%, is from dry smoke deposition. This finding is also supported by the fact that there was little
296 precipitation during this time based on the NAAPS modeled meteorology (Fig. 5B), but it is also
297 important to note that snow aging could also play a role in aggregation of BC particles. The
298 decrease observed in the surface hoar rBC concentrations in the August 11th samples may
299 suggest there was a process that removed the particles from the surface hoar, such as flushing or
300 redistribution by supra-glacial melt, or uncontaminated fresh snow deposition which could dilute
301 the concentrations. Further investigation into this process is warranted.



302



303

304 **Figure 5:** A) Biomass burning derived smoke deposition flux separated as wet and dry
 305 deposition and B) total precipitation produced by the NAAPS model. The total smoke deposition
 306 closely follows the wet deposition line. The five sampling dates are marked in orange.

307

308 4 Conclusion

309 Here we present (to the author's knowledge) the first rBC size distributions from fresh snow
 310 and surface hoar in the bare ice region of the GrIS, coupled with their concentrations. An initial
 311 rBC size distribution in a fresh snow sample from the GrIS shows pronounced bimodality and
 312 very large particles with the second peak almost 2 μm . These initial rBC size distributions from
 313 surface hoar in the bare ice dark zone of the Greenland Ice Sheet are smaller than the fresh snow,
 314 but still much larger than observations of atmospheric rBC. There appears to be a shift in the

315 modal peak of rBC particle size in light patches over the duration of the season from $\sim 0.3 \mu\text{m}$ to
316 $\sim 1.4 \mu\text{m}$, further suggesting aggregation of particles in the bare-ice region. NAAPS-AOT and
317 surface concentration data suggest that rBC surface hoar concentrations in the bare ice zone
318 reflect atmospheric conditions momentarily, before possibly being reset by supra-glacial melt.

319 Additionally, we demonstrate preliminary verification of BC deposition from the NAAPS-
320 RA with *in-situ* observations. rBC measurements in dark patches from late June to early August
321 2014 reveal an increase just after the smoke event. These elevated concentrations are closer to
322 previously reported values in vertical snow and ice-core layers (e.g., Doherty et al., 2010 and
323 Polashenski et al., 2013). The overall higher concentrations of rBC in visibly darker patches,
324 where higher concentrations of ice algae were observed (Stibal et al., 2017), suggest potential bio
325 flocculation with ice algae and mineral dust. However, NAAPS model results also indicate the
326 increase is likely related to accumulation of episodically deposited wildfire-derived smoke. For
327 example, the smoke event in early August, which brought smoke from the western Northern
328 Hemisphere. Based on NAAPS deposition model and corroborated by rBC observations, wet
329 deposition appears to be the largest source of rBC to the surface. For example, our fresh snow
330 sample was measured at $3 \mu\text{g-rBC/L-H}_2\text{O}$, while the model, off by a factor of 7, produced $21 \mu\text{g-}$
331 $\text{rBC/L-H}_2\text{O}$. These preliminary results suggest global aerosol models may be overestimating BC
332 deposition; however, further investigation is warranted. These data provide utility in
333 understanding the seasonal evolution of impurities, which are needed to constrain modeling of
334 ice-albedo feedbacks in the bare-ice zone of the GRIS.

335

336 **Author Contributions**

337 ALK and JS analyzed the rBC samples. PX ran the NAAPS model and provided output data.
338 ALK wrote the manuscript and PX and JS edited and contributed text. The samples were
339 collected by ALK and the Dark Snow Project.

340 **Acknowledgements**

341 The authors thank the Dark Snow Project for field support and additional sample collection,
342 specifically, M. Stibal, J. Box and K. Cameron and N. Molotch.

343
344 **Competing Interests.** There are no conflicts of interest.

345 346 **Data Availability**

347 **The rBC and NAAPS modeled deposition data are included in Table 1.**

348 349 **References**

- 350 Baumgardner, D., Popovicheva, O., Allan, J., Bernardoni, V., Cao, J., Cavalli, F., et al. (2012).
351 Soot reference materials for instrument calibration and intercomparisons : a workshop
352 summary with recommendations. 1869–1887. doi:10.5194/amt-5-1869-2012.
- 353 Bond, T. C., Doherty, S. J., Fahey, D. W., Forster, P. M., Berntsen, T., DeAngelo, B. J., et al.
354 (2013). Bounding the role of black carbon in the climate system: A scientific assessment. *J.*
355 *Geophys. Res. Atmos.* 118, 5380–5552. doi:10.1002/jgrd.50171.
- 356 Cordero, R. R., Sepúlveda, E., Feron, S., Damiani, A., Fernandoy, F., Neshyba, S., ... & Casassa,
357 G. (2022). Black carbon footprint of human presence in Antarctica. *Nature*
358 *communications*, 13(1), 1-11.
- 359 Doherty, S. J., Grenfell, T. C., Forsström, S., Hegg, D. L., Brandt, R. E., and Warren, S. G.
360 (2013). Observed vertical redistribution of black carbon and other insoluble light-absorbing
361 particles in melting snow. *J. Geophys. Res. Atmos.* 118, 5553–5569.
362 doi:10.1002/jgrd.50235.
- 363 Doherty, S. J., Warren, S. G., Grenfell, T. C., Clarke, a. D., and Brandt, R. E. (2010a). Light-
364 absorbing impurities in Arctic snow. *Atmos. Chem. Phys.* 10, 11647–11680.

365 doi:10.5194/acp-10-11647-2010.

366 Doherty, S. J., Warren, S. G., Grenfell, T. C., Clarke, A. D., and Brandt, R. E. (2010b). and
367 Physics Light-absorbing impurities in Arctic snow. 11647–11680. doi:10.5194/acp-10-
368 11647-2010.

369 Flanner, M. G., Zender, C. S., Randerson, J. T., and Rasch, P. J. (2007). Present-day climate
370 forcing and response from black carbon in snow. *J. Geophys. Res.* 112, D11202.
371 doi:10.1029/2006JD008003.

372 Greuell, W. (2000). Melt-water accumulation on the surface of the Greenland ice sheet: Effect on
373 albedo and mass balance. *Geogr. Ann. Ser. A Phys. Geogr.* 82, 489–498.
374 doi:10.1111/j.0435-3676.2000.00136.x.

375 Hanna, E., Huybrechts, P., Steffen, K., Cappelen, J., Huff, R., Shuman, C., et al. (2008).
376 Increased runoff from melt from the Greenland Ice Sheet: A response to global warming. *J.*
377 *Clim.* 21, 331–341. doi:10.1175/2007JCLI1964.1.

378 Katich, J. M., A. E. Perring, and J. P. Schwarz (2017), Optimized detection of particulates from
379 liquid samples in the aerosol phase: focus on black carbon, *Aeros. Sci. Technol.*,
380 doi:10.1080/02786826.2017.1280597

381 Keegan, K. M., Albert, M. R., McConnell, J. R., and Baker, I. (2014a). Climate change and forest
382 fires synergistically drive widespread melt events of the Greenland Ice Sheet. 1–4.
383 doi:10.1073/pnas.1405397111.

384 Keegan, K. M., Albert, M. R., McConnell, J. R., and Baker, I. (2014b). Climate change and
385 forest fires synergistically drive widespread melt events of the Greenland Ice Sheet. *Proc.*
386 *Natl. Acad. Sci. U. S. A.* 111. doi:10.1073/pnas.1405397111.

387 Khan, A. L., McMeeking, G. R., Schwarz, J. P., Xian, P., Welch, K. A., Berry Lyons, W., &

388 McKnight, D. M. (2018). Near-surface refractory black carbon observations in the
389 atmosphere and snow in the McMurdo dry valleys, Antarctica, and potential impacts of
390 Foehn winds. *Journal of Geophysical Research: Atmospheres*, 123(5), 2877-2887.

391 Khan, A. L., H. Dierssen, J. P. Schwarz, C. Schmitt, A. Chlus, M. Hermanson, T. H. Painter,
392 and D. M. M. (2017). “Impacts of coal dust on the spectral reflectance of Arctic surface
393 snow in Svalbard, Norway”, *Journal of Geophysical Research: Atmospheres*, 1–12.
394 doi:10.1002/2016JD025757.

395 Khan, A.L., Wagner, S., Jaffe, R., Xian P. , Williams M., and Armstrong, R., and McKnight, D.
396 (2017). “Dissolved black carbon in the global cryosphere: Concentrations and chemical
397 signatures”, *Geophysical Research Letters*, 1–9. doi:10.1002/2017GL073485.

398 Lewis, G., Osterberg, E., Hawley, R., Marshall, H. P., Meehan, T., Graeter, K., et al. (2021).
399 Atmospheric blocking drives recent albedo change across the western Greenland ice sheet
400 percolation zone. *Geophysical Research Letters*, 48, e2021GL092814.
401 <https://doi.org/10.1029/2021GL092814>

402 Lim, S., Fain, X., Zanatta, M., Cozic, J., Jaffrezo, J.-L., Ginot, P., et al. (2014). Refractory black
403 carbon mass concentrations in snow and ice: method evaluation and inter-comparison with
404 elemental carbon measurement. *Atmos. Meas. Tech.* 7, 3549–3589. doi:10.5194/amtd-7-
405 3549-2014.

406 Lynch, P., Reid, J. S., Westphal, D. L., Zhang, J., Hogan, T. F., Hyer, E. J., Curtis, C. A., Hegg,
407 D. A., Shi, Y., Campbell, J. R., Rubin, J. I., Sessions, W. R., Turk, F. J., and Walker, A. L.:
408 An 11-year global gridded aerosol optical thickness reanalysis (v1.0) for atmospheric and
409 climate sciences, *Geosci. Model Dev.*, 9, 1489–1522, [https://doi.org/10.5194/gmd-9-1489-](https://doi.org/10.5194/gmd-9-1489-2016)
410 2016, 2016.

411 Markowicz, K. M., et al. (2016), Impact of North American intense fires on aerosol optical

412 properties measured over the European Arctic in July 2015, *J. Geophys. Res. Atmos.*, 121,
413 14,487–14,512, doi:10.1002/2016JD025310.

414 Markowicz, K.M., Lisok, J., Xian, P., Simulation of long-term direct aerosol radiative forcing
415 over the arctic within the framework of the iAREA project, *Atmospheric Environment*
416 (2021), doi: <https://doi.org/10.1016/j.atmosenv.2020.117882>.

417 McConnell, J. R., Edwards, R., Kok, G. L., Flanner, M. G., Zender, C. S., Saltzman, E. S., et al.
418 (2007a). 20th-century industrial black carbon emissions altered Arctic climate forcing.
419 *Science (80-.)*. 317, 1381–4. doi:10.1126/science.1144856.

420 McConnell, J. R., Edwards, R., Kok, G. L., Flanner, M. G., Zender, C. S., Saltzman, E. S., et al.
421 (2007b). 20th-Century Industrial Black Carbon Emissions Altered Arctic Climate Forcing.
422 *Science (80-.)*. 317, 1381 LP – 1384. doi:10.1126/science.1144856.

423 Mori, T., Goto-Azuma, K., Kondo, Y., Ogawa-Tsukagawa, Y., Miura, K., Hirabayashi, M., et al.
424 (2019). Black Carbon and Inorganic Aerosols in Arctic Snowpack. *J. Geophys. Res. Atmos.*,
425 2019JD030623. doi:10.1029/2019JD030623.

426 Polashenski, C. M., Dibb, J. E., Flanner, M. G., Chen, J. Y., Courville, Z. R., Lai, A. M., et al.
427 (2015a). Neither dust nor black carbon causing apparent albedo decline in Greenland’s dry
428 snow zone: Implications for MODIS C5 surface reflectance. 9319–9327.
429 doi:10.1002/2015GL065912.Received.

430 Polashenski, C. M., Dibb, J. E., Flanner, M. G., Chen, J. Y., Courville, Z. R., Lai, A. M., et al.
431 (2015b). Neither dust nor black carbon causing apparent albedo decline in Greenland’s dry
432 snow zone: Implications for MODIS C5 surface reflectance. *Geophys. Res. Lett.* 42.
433 doi:10.1002/2015GL065912.

434 Ranjbar, K., O’Neill, N. T., Lutsch, E., McCullough, E. M., AboEl-Fetouh, Y., Xian, P., et al.

435 (2019). Extreme smoke event over the high Arctic. *Atmos. Environ.* 218, 117002.
436 doi:<https://doi.org/10.1016/j.atmosenv.2019.117002>.

437 Reid, J. S., Koppmann, R., Eck, T. F., and Eleuterio, D. P.: A review of biomass burning
438 emissions part II: intensive physical properties of biomass burning particles, *Atmos. Chem.*
439 *Phys.*, 5, 799–825, <https://doi.org/10.5194/acp-5-799-2005>, 2005.

440 Ryan, J. C., Hubbard, A., Stibal, M., Irvine-Fynn, T. D., Cook, J., Smith, L. C., et al. (2018).
441 Dark zone of the Greenland Ice Sheet controlled by distributed biologically-active
442 impurities. *Nat. Commun.* 9, 1–10. doi:10.1038/s41467-018-03353-2.

443 Ryan, J. C., Smith, L. C., Van As, D., Cooley, S. W., Cooper, M. G., Pitcher, L. H., et al. (2019).
444 Greenland Ice Sheet surface melt amplified by snowline migration and bare ice exposure.
445 *Sci. Adv.* 5, 1–11. doi:10.1126/sciadv.aav3738.

446 Schwarz, J. P., Doherty, S. J., Li, F., Ruggiero, S. T., Tanner, C. E., Perring, a. E., et al. (2012).
447 Assessing recent measurement techniques for quantifying black carbon concentration in
448 snow. *Atmos. Meas. Tech. Discuss.* 5, 3771–3795. doi:10.5194/amtd-5-3771-2012.

449 Schwarz, J. P., Gao, R. S., Perring, a E., Spackman, J. R., and Fahey, D. W. (2013). Black
450 carbon aerosol size in snow. *Sci. Rep.* 3, 1356. doi:10.1038/srep01356.

451 Stibal, M., Box, J. E., Cameron, K. A., Langen, P. L., Yallop, M. L., M., H., R., Khan, A.L.,
452 Molotch, N. P., Christmas, N.A.M., Quaglia, F.C., , Remias, D., Paul, C.J.P., Van den
453 Broeke, M., Ryan, J., Hubbard, A., Tranter, M., van As, D., and and Ahlstrøm, A. (2017).
454 Algae Drive Enhanced Darkening of Bare Ice on the Greenland Ice Sheet. *Geophys. Res.*
455 *Lett.*, 463–471. doi:10.1002/2017GL075958.

456 Stibal, M., Elster, J., Šabacká, M., and Kaštovská, K. (2007). Seasonal and diel changes in
457 photosynthetic activity of the snow alga *Chlamydomonas nivalis* (Chlorophyceae) from

458 Svalbard determined by pulse amplitude modulation fluorometry. *FEMS Microbiol. Ecol.*
459 59, 265–273. doi:10.1111/j.1574-6941.2006.00264.x.

460 Tedesco, M., Doherty, S., Fettweis, X., Alexander, P., Jeyaratnam, J., Noble, E., et al. (2016).
461 The darkening of the Greenland ice sheet: trends, drivers and projections
462 (1981–2100). *Cryosph.* 9, 5595–5645. doi:10.5194/tcd-9-5595-2015.

463 Wendl, I. a., Menking, J. a., Färber, R., Gysel, M., Kaspari, S. D., Laborde, M. J. G., et al.
464 (2014). Optimized method for black carbon analysis in ice and snow using the Single
465 Particle Soot Photometer. *Atmos. Meas. Tech.* 7, 3075–3111. doi:10.5194/amtd-7-3075-
466 2014.

467 Wientjes, I. G. M., Van De Wal, R. S. W., Reichert, G. J., Sluijs, A., and Oerlemans, J. (2011).
468 Dust from the dark region in the western ablation zone of the Greenland ice sheet.
469 *Cryosphere* 5, 589–601. doi:10.5194/tc-5-589-2011.

470
471 Xian, P., Zhang, J., O'Neill, N. T., Toth, T. D., Sorenson, B., Colarco, P. R., Kipling, Z., Hyer, E.
472 J., Campbell, J. R., Reid, J. S., and Ranjbar, K.: Arctic spring and summertime aerosol
473 optical depth baseline from long-term observations and model reanalyses – Part 1:
474 Climatology and trend, *Atmos. Chem. Phys.*, 22, 9915–9947, [https://doi.org/10.5194/acp-](https://doi.org/10.5194/acp-22-9915-2022)
475 [22-9915-2022](https://doi.org/10.5194/acp-22-9915-2022), 2022.

476 Xian, P., Zhang, J., O'Neill, N. T., Reid, J. S., Toth, T. D., Sorenson, B., Hyer, E. J., Campbell, J.
477 R., and Ranjbar, K.: Arctic spring and summertime aerosol optical depth baseline from
478 long-term observations and model reanalyses – Part 2: Statistics of extreme AOD events,
479 and implications for the impact of regional biomass burning processes, *Atmos. Chem.*
480 *Phys.*, 22, 9949–9967, <https://doi.org/10.5194/acp-22-9949-2022>, 2022.

481